

Annual Review of Chemical and Biomolecular Engineering

Electrochemical Manufacturing Routes for Organic Chemical Commodities

Ricardo Mathison, Alexandra L. Ramos Figueroa, Casey Bloomquist, and Miguel A. Modestino

Department of Chemical and Biomolecular Engineering, New York University, Brooklyn, New York, USA; email: mathison@nyu.edu, arf426@nyu.edu, bloomquist@nyu.edu, modestino@nyu.edu

Annu. Rev. Chem. Biomol. Eng. 2023. 14:9.1-9.24

The Annual Review of Chemical and Biomolecular Engineering is online at chembioeng.annualreviews.org

https://doi.org/10.1146/annurev-chembioeng-101121-090840

Copyright © 2023 by the author(s). All rights reserved

Keywords

organic electrosynthesis, electrochemistry, chemical manufacturing, electrification, decarbonization

Abstract

Electrochemical synthesis of organic chemical commodities provides an alternative to conventional thermochemical manufacturing and enables the direct use of renewable electricity to reduce greenhouse gas emissions from the chemical industry. We discuss electrochemical synthesis approaches that use abundant carbon feedstocks for the production of the largest petrochemical precursors and basic organic chemical products: light olefins, olefin oxidation derivatives, aromatics, and methanol. First, we identify feasible routes for the electrochemical production of each commodity while considering the reaction thermodynamics, available feedstocks, and competing thermochemical processes. Next, we summarize successful catalysis and reaction engineering approaches to overcome technological challenges that prevent electrochemical routes from operating at high production rates, selectivity, stability, and energy conversion efficiency. Finally, we provide an outlook on the strategies that must be implemented to achieve large-scale electrochemical manufacturing of major organic chemical commodities.



INTRODUCTION

The chemical manufacturing sector accounts for approximately 5% of the primary energy use in the United States (4,842 TBTU in 2018) and 5% of greenhouse gas (GHG) emissions (332 MMT CO₂ equivalents) (1). Emissions from this sector arise primarily from the use of fossil fuelderived heat to drive thermochemical reaction and separation processes. An emerging strategy to decarbonize chemical manufacturing involves the use of emissions-free electricity from wind, solar, nuclear, or hydroelectrical power sources to drive these processes. This electrification strategy can be achieved through a combination of approaches including plant retrofits to replace fossil fuel combustion with electrical heating and electrolytic hydrogen combustion (2). These shortterm approaches could achieve decarbonization of on-site chemical plant operations but likely would not improve the efficiency of state-of-the-art thermal processes. Long-term electrification strategies based on emerging electrochemical manufacturing technologies can provide additional benefits over thermal processes (3–7), but these technologies are at an early stage of development. Potential benefits from electrochemical manufacturing technologies include (a) precise control of selectivity via potential modulation, (b) operation at mild temperatures and pressures, (c) easy usage of distributed renewable chemical feedstocks due to the modular nature of electrochemical reactors, (d) minimized chemical waste by avoiding the need for chemical oxidants or reducing reagents, and (e) the ability to perform coupled oxidation and reduction reactions in a single reactor. Substantial advances from research and development are required to benefit from these potential advantages at the scales required for chemical manufacturing.

We review the state of the art of electrochemical approaches to produce the largest petrochemical precursors and basic organic chemical products: light olefins, olefin oxidation derivatives, aromatics, and methanol (**Figure 1**). These product classes account for a substantial fraction of the energy utilization in the chemical industry (37% of on-site energy consumption in the United States in 2015) (8), and decarbonizing their production will have a significant impact on GHG emissions. While this review focuses on organic chemical commodities with viable electrochemical production routes, other product classes with a significant carbon footprint will also need to be decarbonized to achieve carbon neutrality in the chemical industry (e.g., ammonia, ethanol, inorganic basic chemicals). Throughout this review, we emphasize electrochemical routes that

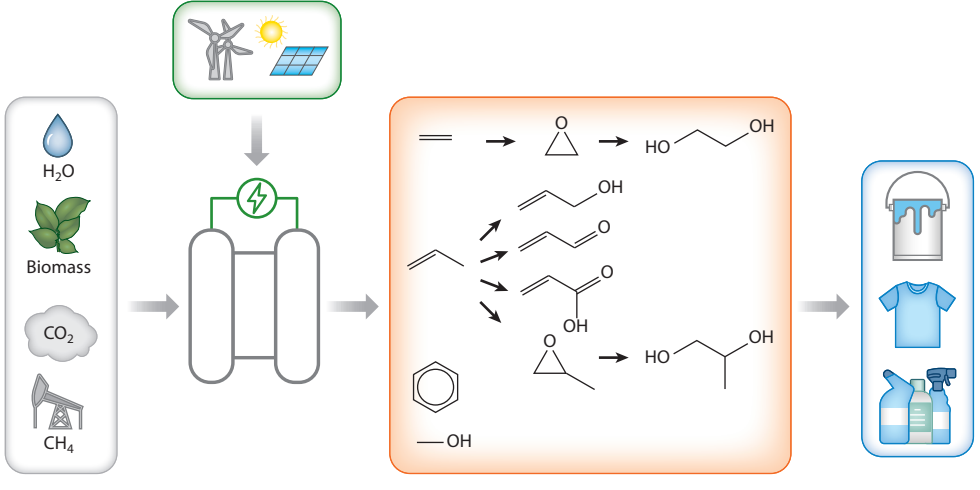


Figure 1

Electrochemical production of high-environmental impact organic chemicals from inexpensive carbon feedstocks that act as precursors to ubiquitous consumer products.

9.2 Mathison et al.



use abundant carbon feedstocks, such as CO₂, biomass, and natural gas, and highlight the research developments required to enable practical deployment of electrochemical manufacturing technologies at scale.

ELECTROCHEMICAL ETHYLENE PRODUCTION

Ethylene is the largest chemical commodity produced in industry. Steam cracking, the most common method for ethylene production, is the most energy-intensive petrochemical process (9). GHG emissions from ethylene production are estimated to be 1.135 and 0.840 kg of CO₂/kg ethylene for steam cracking of naphtha and ethane, respectively (10). Approximately 90% of these emissions are linked to the energy requirements of the endothermic reactions involved (9). In addition, a substantial source of GHG emissions for the thermochemical production of ethylene comes from the energy requirement in the downstream paraffin–olefin separations. Below, we describe alternative electrochemical routes to generate ethylene.

CO₂ to Ethylene

Low-temperature CO_2 electroreduction to ethylene is the most-studied electrochemical ethylene production route. This section summarizes important advances in the understanding and practical implementation of the CO_2 reduction reaction (CO_2RR), and the reader is referred to recent reviews on the topic for an in-depth assessment of the field (11–14). Under standard conditions, the reduction of CO_2 to ethylene requires a minimum change of Gibbs free energy of $\Delta G_{rxn}^{\circ} = 1,331$ kJ/mol C_2H_4 (Equation 1) and a total of 12 electron-transfer steps:

$$2CO_2 + 2H_2O \rightarrow C_2H_4 + 3O_2$$
, $\Delta G_{rxn} = 1{,}331 \text{ kJ/mol}C_2H_4$.

Hori et al. (15) initially explored the activity of different metal electrocatalysts and demonstrated the ability of Cu to reduce CO₂ to ethylene and other products that require more than two electron transfers at high Faradaic efficiencies (FE)—a finding that has been corroborated by several studies (16–19). The exceptional activity of Cu toward the reduction of CO₂ to C₂₊ products, such as ethylene, arises from its unique ability to balance the binding energies of CO₂RR and hydrogen evolution reaction (HER) intermediates. Bagger et al. (20) classified several metals based on their CO₂RR activity and established that Cu was the only electrocatalyst with a negative adsorption energy for adsorbed CO (*CO) and a positive adsorption energy for adsorbed hydrogen (*H), as shown in **Figure 2a**. The strong *CO adsorption energy promotes CO₂RR to ethylene, as the dimerization of *CO to *C₂O₂ is believed to be the rate-determining step (21) (**Figure 3**). Also, the relatively weak adsorption of *H suppresses the competing HER rates.

Given that CO₂RR performance is highly dependent on the balance of adsorption energies of intermediates, the research community has explored multimetallic electrocatalysts to modulate surface energy profiles (22, 23). Although this is a promising research direction, to date, there have been no demonstrations of multimetallic catalysts that outperform the intrinsic activity of Cu toward ethylene production (11, 24). An alternative strategy to enhance ethylene selectivity is to modulate the electrocatalyst microenvironment (e.g., concentration, size, and polarity of supporting ions; modification of electrode surfaces with organic thin films; and modulation of local pH) to control the concentration of reactive species and intermediates at the electrode–electrolyte interface. Using large supporting cations (e.g., Cs⁺) (25) and maintaining a local alkaline pH near the catalysts lead to an increased selectivity toward C₂₊ products (26, 27). Incorporating organic films, such as ion-conducting polymer films (ionomers), can help control local solubility of CO₂; transport properties of reactants, products, and intermediates; and maintain local alkaline pH profiles that are favorable for ethylene production (28–30). For example, Chen et al. (28) introduced polymer thin films at the interface of the Cu electrode and demonstrated ethylene FE



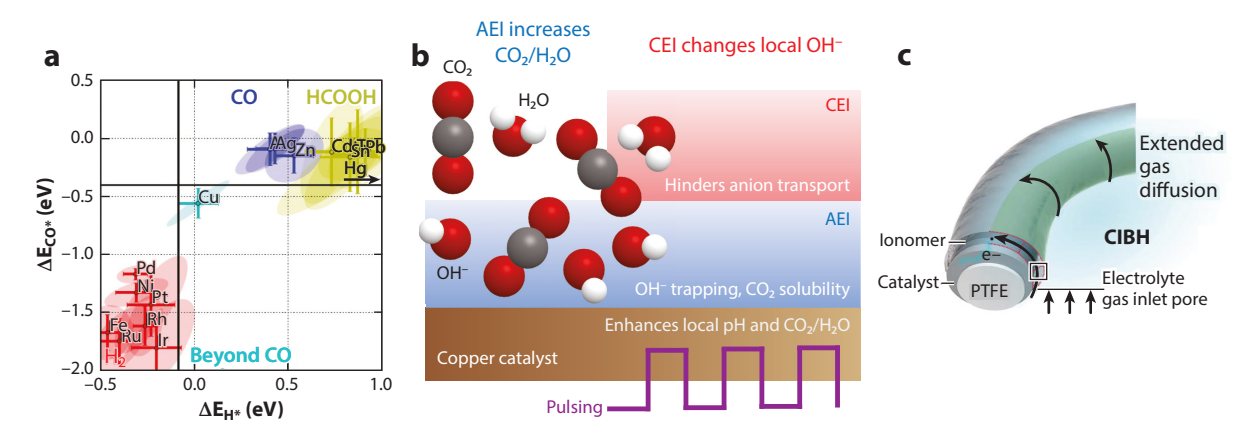


Figure 2

Recent discoveries and advances in CO₂ electroreduction to ethylene. (a) CO₂ reduction metal classification based on their hydrogen and CO adsorption energy. Panel adapted with permission from Reference 20; copyright 2017 John Wiley and Sons. (b) Schematic illustration of enhanced CO₂RR using ionomers. Bilayer CEI and AEI coatings and dosing of potential via pulsed electrolysis are responsible for maintaining high local concentration of CO₂ and OH⁻ ions. Panel adapted with permission from Reference 30. (c) Schematic of the CIBH. Metal catalyst is deposited onto a PTFE hydrophobic fiber support that promotes gas transport, whereas water and ion transport are facilitated by the hydrophilic ionomer. Panel adapted with permission from Reference 36. Abbreviations: AEI, anion-exchange ionomer; CEI, cation-exchange ionomer; CIBH, catalyst:ionomer bulk heterojunction; CO₂RR, CO₂ reduction reaction; PTFE, polytetrafluoroethylene.

of up to 87% at -0.47 V. Li et al. (29) studied a broad library of polymeric thin films derived from N-arylpyridinium and demonstrated that increasing the number of nitrogen sites stabilized *CO on the Cu surface, resulting in an ethylene FE of up to 72%. Kim et al. (30) conducted studies on electrodes modified with bilayer cation— and anion—exchanged ionomer coatings (CEI and AEI, respectively). Under this configuration, the AEI layer increased local pH at the interface with the catalyst, whereas the CEI layer prevented the migration of OH $^-$ ions from the AEI—catalyst interface to the bulk, supporting a stable alkaline environment near the electrode, as depicted in **Figure 2b**. Furthermore, dynamic dosing of potential via pulsed electrolysis maintained a high concentration of CO₂ and OH $^-$ ions at the catalyst interface, enhancing C₂₊ FE up to 89% from 78% for static electrolysis (31). These results demonstrate the importance of regulating microenvironments around the electrocatalysts to control ethylene selectivity.

Implementing the catalytic CO₂ electroreduction advances in scalable devices requires the operation of electrochemical cells at high current densities and over extended periods of time. Strategies to improve the production rate of such devices include nanostructuring electrodes to increase their electrochemically active surface area (ECSA) and increasing the flux of CO₂ to the surface of the catalyst to mitigate mass transport limitations (32). Given the low solubility of CO₂ in electrolytes, the behavior of CO₂RR cells at high current densities depends greatly on the interplay between CO₂ mass transport rates and intrinsic CO₂RR kinetics (11). To achieve high ethylene production rates, the ECSA of the electrodes should be designed to achieve high CO₂RR current densities at overpotentials that promote ethylene formation (usually in the range of 0.9–1.1 V for planar electrodes), rather than other products (e.g., hydrogen, methane, CO, or formate). One of the largest challenges at high current densities is maintaining a sufficiently high flux of CO₂ to the electrode surface to mitigate mass transport limitations. Also of note, the higher desirable current densities increase the proton reduction rate, thus raising the local pH at the electrode–electrolyte interface, promoting ethylene formation, and suppressing HER (33). Strategies that increase mixing between CO₂ streams and electrolytes can increase the rate

9.4 Mathison et al.



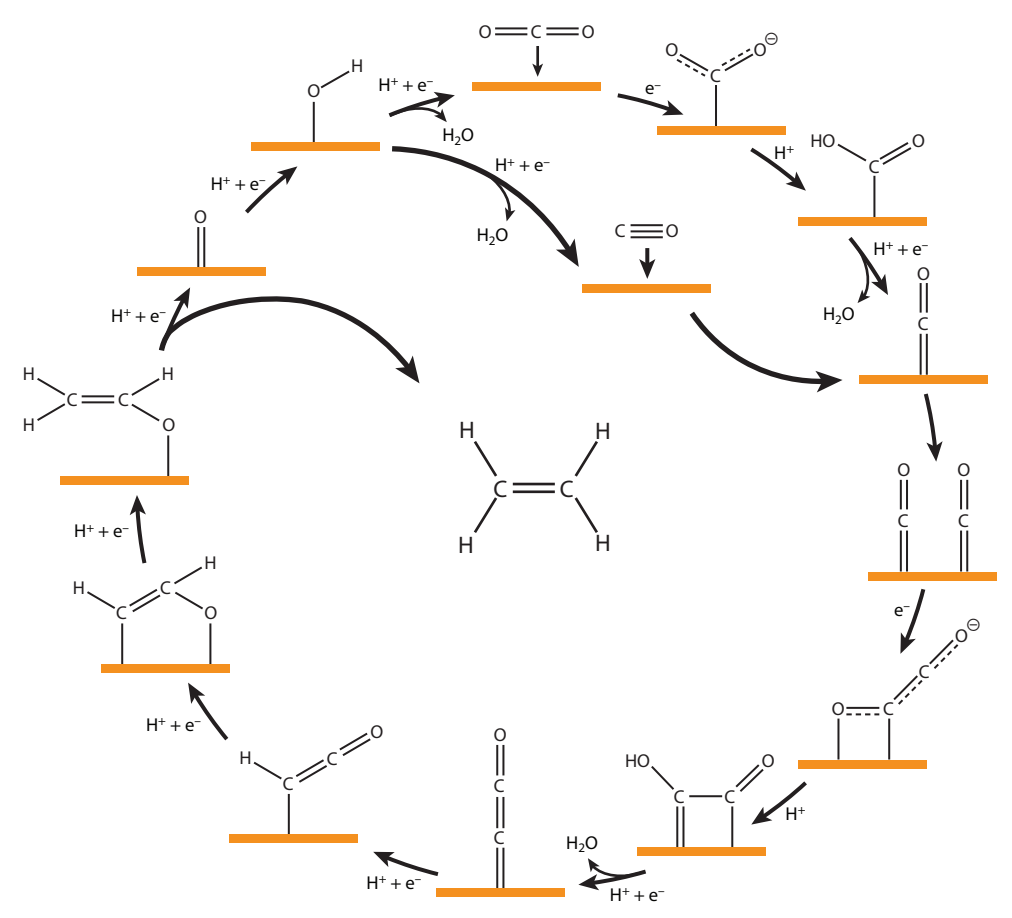


Figure 3

Proposed reaction mechanism for the electrocatalytic reduction of CO_2 and CO to ethylene on transition metals catalysts. Figure adapted with permission from Reference 21; copyright 2015 American Chemical Society.

of CO_2RR , circumventing mass transport limitations (34). The implementation of gas diffusion electrodes (GDEs) to control the three-phase interface between CO_2 , Cu, and electrolyte can substantially enhance the CO_2 mass transport rates and maximize the ECSA (35). GDE-based flow devices composed of catalyst/ionomer bulk heterojunctions (**Figure 2***c*) have demonstrated >65% ethylene FE (36). These devices operate stably for more than 60 h at commercially relevant current densities (i.e., >1 A cm⁻²). These recent demonstrations were possible due to the accelerated advances in CO_2 electroreduction over the past decade and have opened up opportunities to develop scale-up strategies for electrochemical ethylene production systems.

CO to Ethylene

Review in Advance first posted on March 17, 2023. (Changes may still occur before final publication.)

CO electroreduction is a promising electrochemical route to produce ethylene at high production rates (Equation 2):

$$2CO + 2H_2O \rightarrow C_2H_4 + 2O_2$$
, $\Delta G_{rxn} = 817 \text{ kJ/mol } C_2H_4$.

The CO reduction reaction (CORR) has several advantages over CO_2RR due to the different behavior of CO and CO_2 in aqueous electrolytes. Whereas CO_2 readily forms inactive carbonates



in alkaline media, CO is stable under such conditions (37). This allows CORR to take place at high pH, promoting ethylene formation and suppressing HER (38). Additionally, whereas CO₂RR to ethylene requires 12 electron transfer steps, CORR requires only 8 steps. The use of CO also avoids the formation of formic acid, a CO₂RR product that requires only 2 electron transfers and substantially lowers the selectivity to C_{2+} products (39).

As with CO_2RR , Cu has an exceptional ability to reduce CO to C_{2+} products such as ethylene. This is because the adsorption of *CO in the electrocatalyst surface is a critical step in the production of ethylene from both CO and CO₂ (26, 40), and the proposed mechanism depicted in Figure 3 follows a similar path to CO₂RR once CO is adsorbed on the surface. Hori et al. (27) reported the first demonstration of CORR toward ethylene at high current densities (i.e., >1 mA cm⁻²). Subsequent studies focused on understanding the product distribution and reaction mechanisms at relatively low current densities (41, 42). These studies, performed in liquid cells, were limited by the poor solubility of CO in aqueous electrolyte. To circumvent this transport limitation, recent studies have implemented GDEs for CORR to enhance the rates of CO transport to the electrocatalyst-electrolyte interface. Han et al. (43) reported one of the first high-current density demonstrations of CORR on GDEs, achieving an ethylene partial current density of 50.8 mA cm⁻². Further studies led to improved performance, with a recent demonstration of a flow GDE-based device with 72% ethylene FE at a current density >800 mA cm⁻² from a feed stream containing 10% CO in N₂ (44). This study found that maintaining an intermediate concentration of CO in the feed stream was important to achieve high ethylene FE, because high availability of CO promoted the formation of oxygenated products (i.e., ethanol, acetate, and 1-propanol), whereas low availability of CO promoted HER.

Given the advantages of CORR over CO₂RR for electrochemical production of ethylene, a two-step system in which CO₂ gets converted to CO and CO is subsequently reduced to multicarbon products may provide a more efficient route to ethylene. Recent studies have demonstrated sequential cascade CO₂ reduction using solid-electrolysis cells (45), GDEs (46), and continuous flow reactors (47) for the CO₂ reduction-to-CO step. Romero Cuellar et al. (46) achieved a 62% total FE for multicarbon products at 300 mA cm⁻² using an Ag GDE in the first step and Cu nanoparticles on a carbon-based diffusion structure to obtain C_{2+} products from CO. In cascade reactor designs, the unreacted CO2 from the first step of the process competes with CO in the second step and must be separated to achieve higher efficiencies.

Light Alkanes to Ethylene

An alternative for ethylene production is to use light hydrocarbons as chemical feedstocks and generate olefins via electrocatalytic dehydrogenation (EDH). Methane and ethane EDH is an advantageous route to ethylene production, compared to CO₂ and CO electroreduction, due to the abundance and low cost of the feedstocks and the lower thermodynamic energy barrier for the transformation. Additionally, methane and ethane EDH may release hydrogen as a reduction coproduct (Equations 3 and 5), or the reaction can be coupled with oxygen reduction in the cathode to further reduce the energy requirement, leading to an exergonic reaction (Equations 4 and 6). In both cases, the required energy input is substantially smaller than the CO₂ and CO reduction reactions discussed in the previous sections.

$$C_2H_6 \rightarrow C_2H_4 + H_2$$
, $\Delta G_{rxn} = 100 \text{ kJ/mol } C_2H_4$.

$$C_2H_6 + \frac{1}{2}O_2 \rightarrow C_2H_4 + H_2O$$
, $\Delta G_{rxn} = -137 \text{ kJ/mol } C_2H_4$.

$$2CH_4 \rightarrow C_2H_4 + 2H_2$$
, $\Delta G_{rxn} = 169 \text{ kJ/mol } C_2H_4$. 5.

$$2CH_4 + O_2 \rightarrow C_2H_4 + 2H_2O$$
, $\Delta G_{rxn} = -305 \text{ kJ/mol } C_2H_4$.

Mathison et al. 9.6



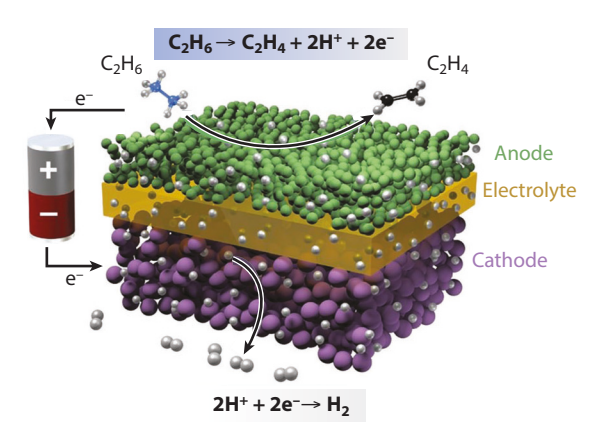


Figure 4

Schematic of the production of ethylene in a solid-oxide electrochemical cell. Protons are transferred from the anode through the perovskite electrolyte membrane to the cathode where H₂ is produced. Figure adapted with permission from Reference 57.

A few demonstrations of light hydrocarbon EDH in solid-oxide electrochemical cells (SOECs) have been reported (48). These involve the dehydrogenation of ethane to ethylene in protonic SOECs (49, 50), where ethane C-H bonds are cleaved in an electrocatalytic layer and released protons migrate through a ceramic conductor [e.g., perovskite proton-conducting oxides, such as BaZr_{0.1}Ce_{0.7}Y_{0.2}O_{3-δ} (BZCY)] to the cathodic side of the cell, where they can be reduced to H₂ (Figure 4) or recombine with an oxidant (e.g., CO₂ or O₂). Alternatively, hydrocarbons can undergo oxidative dehydrogenation in an oxygen ion-conducting electrolyte where oxide ions (O²⁻) are generated on the cathode catalyst and transported to the anode surface through a dense solid oxide electrolyte to react with alkanes to generate olefins and water (51). The advantages of these electrocatalytic processes over the thermo-catalytic dehydrogenation and oxidative dehydrogenation are that (a) the presence of oxide ions in the reaction chamber lifts the thermodynamic limitation of the direct dehydrogenation; (b) hydrocarbons and gas-phase oxygen never come in contact with each other, hence reducing the possibility of further oxidation to CO_2 ; (c) oxide ions help to gasify/oxidize any carbonaceous species that may deposit on the anode catalyst surface and cause deactivation (e.g., via coking); and (d) the surface properties of the anode materials can be tuned to enhance desorption of olefins before they encounter oxygen ions (52).

Oxygen ion–conducting electrolyte cells contain a solid oxide electrolyte sandwiched between the catalytic anodic and cathodic layers that serve as electrodes. The solid electrolyte should have a high oxygen ion conductivity but low electrical conductivity (53). The most commonly used material for oxygen ion–conducting electrolytes is zirconia doped with larger cations (e.g., yttriastabilized zirconia), which exhibits high ionic conductivity at moderate and high temperatures (600–1,000°C) (54).

Proton-conducting ceramics have several advantages over oxygen ion–conducting ceramics. The smaller size of the protonic charge carrier leads to a larger ionic conductivity, which drives better performance at lower operating temperatures (450–600°C) (55). Additionally, proton-conducting ceramics exhibit reliable performance and durability when exposed to a broad range of hydrocarbon fuels (56). The most ubiquitous proton-conducting ceramics are ABO₃ perovskites based on Ba, Ce, and Zr, where Ba occupies the A site and Ce and/or Zr occupy the B site in these structures (55). Out of these ceramics, BCZYYb was demonstrated to achieve a high ionic conductivity (6.2 10⁻³ S cm⁻¹) at low operating temperature (400°C) and close to 100%



selectivity toward ethylene via ethane deprotonation at a constant current density of 1 A cm⁻² (57). This study was followed by a detailed process simulation using Aspen Plus software, in which low-temperature electrochemical nonoxidative deprotonation of ethane was shown to be economically and environmentally superior to steam cracking (58).

Electrocatalysts are integrated directly with SOEC cells to promote ethylene production. Zhu et al. (48) classified electrocatalysts for protonic SOECs into three categories: (a) metals, (b) nanocomposites of transition metals and oxides, and (c) transition-metal alloy nanoparticles. Metals (e.g., Pt, Ni) often show a high activity toward C-H bond activation (48), but they often lead to carbon deposition from further alkane dehydrogenation. In contrast, nanocomposites of transition metals and oxides block undesired side reactions, such as coke formation or ethane isomerization, leading to stabler and more efficient ethylene synthesis. Some common examples of these catalysts are Co–Cr₂O₃, Cu–Cr₂O₃, and FeCr₂O₄, which are highly resistant to coking even at high temperatures and still exhibit ethylene selectivity of >90% (59). Lastly, transition alloy nanoparticles could balance absorption energies of reaction intermediates and, in this way, control product selectivity. For example, EDH demonstrations with Ni_{0.5}Cu_{0.5} alloy nanoparticles have led to >75% ethane conversion and 100% ethylene selectivity at 0.8 V (50).

Electrocatalysts for oxygen ion–conducting electrolytes are classified into two types: (a) multifunctional oxide materials and (b) perovskite doping metal or metal oxides. Multifunctional oxide materials commonly have Mn and W as host oxides and include dopants that enhance ethylene selectivity and/or catalyst activity due to morphological alterations (60). Alternatively, perovskites doped with metal or metal oxides (e.g., Fe/Ag or Al₂O₃) show robust metal-oxide interface interactions that improve active oxygen transfer. For example, Zhu et al. (51) implemented an oxygen ion SOEC for methane oxidation using a $Sr_2Fe_{1.575}Mo_{0.5}O_{6-\delta}$ catalyst and achieved a C_2 selectivity of 82.2% with no degradation after 100 h of operation at high temperatures (850°C).

Evidence in the literature indicates that both methane and ethane can be electrochemically oxidized to ethylene using SOECs. Methane presents an advantage over ethane because it is a more abundant and less expensive feedstock. However, methane generally exhibits a lower conversion toward ethylene, compared to ethane, due to its stronger C-H bonds, which require a higher operating temperature. Additionally, methane requires appropriate catalytic sites for successful C-C coupling from adsorbed *CH₃ species that are generated.

Biomass-Derived Carboxylic Acids to Olefins

Renewable biomass feedstocks can lower the sector's dependence on fossil-derived chemical feedstocks. There are several ways that biomass can be converted into chemicals, including chemocatalytic, enzymatic, and thermochemical reactions (61), but the conventional methods often include temperatures well above 100°C and harsh oxidizing and reducing agents. Alternatively, biomass can be transformed electrocatalytically under mild operating conditions (ambient temperature and pressure) with water as a solvent and hydrogen source, thus enabling the use of renewable electricity sources in chemical manufacturing (62).

Lignocellulosic biomass is a sustainable feedstock for synthesis of renewable carboxylic acids (63). Electro-decarboxylation of these organic acids has been studied for more than a century, beginning with Hermann Kolbe's identification of the formation of alkanes and CO₂ from carboxylic acids. Since then, multiple electro-decarboxylation routes to produce paraffins, olefins, and alcohols have been described (64, 65). The electro-decarboxylation of carboxylic acids follows three distinct pathways (66): Kolbe electrolysis, non-Kolbe electrolysis, and esterification and deep oxidation, as illustrated in **Figure 5**. Each pathway begins with the deprotonation of the carboxylic acid and subsequent electron transfer from the carboxylate to the anode, with

9.8 Mathison et al.



$$\begin{array}{c} \text{Alkane} + \text{alkene} & \begin{array}{c} \text{Alcohol} \\ \text{(non-Kolbe product)} \end{array} \\ \text{Disproportionation} & \begin{array}{c} R \\ \\ R \\ \end{array} & \begin{array}{c} + \\ R \\ \end{array} & \begin{array}{c} R \\ \\ \end{array} & \begin{array}{c} \text{OH} \\ \end{array} & \begin{array}{c} \text{Deep oxidation products} \end{array} \\ \text{Carboxylic acid} & \begin{array}{c} \text{Carboxyl-radical} & \text{Alky-radical} & \text{Carbo-cation } \\ R \\ \end{array} & \begin{array}{c} \text{OH} \\ \end{array} & \begin{array}{c} -H^+ \\ -e^- \end{array} & \begin{array}{c} -CO_2 \\ \end{array} & \begin{array}{c} R \\ \end{array} & \begin{array}{c} CH_2 \\ \end{array} & \begin{array}{c} -e^- \\ \end{array} & \begin{array}{c} R \\ \end{array} & \begin{array}{c} CH_2 \\ \end{array} & \begin{array}{c} -e^- \\ \end{array} & \begin{array}{c} R \\ \end{array} & \begin{array}{c} CH_2 \\ \end{array} & \begin{array}{c} -H^+ \\ \end{array} & \begin{array}{c} R \\ \end{array} & \begin{array}{c} O \\ \end{array} & \begin{array}{c} R \\ \end{array} & \begin{array}{c} O \\ \end{array} & \begin{array}{c} R \\ \end{array} & \begin{array}{c} O \\ \end{array} & \begin{array}{c} R \\ \end{array} & \begin{array}{c} O \\ \end{array} & \begin{array}{c} R \\ \end{array} & \begin{array}{c} O \\ \end{array} & \begin{array}{c} R \\ \end{array} & \begin{array}{c} O \\ \end{array} & \begin{array}{c} R \\ \end{array} & \begin{array}{c} O \\ \end{array} & \begin{array}{c} R \\ \end{array} & \begin{array}{c} O \\ \end{array} & \begin{array}{c} R \\ \end{array} & \begin{array}{c} O \\ \end{array} & \begin{array}{c} O \\ \end{array} & \begin{array}{c} R \\ \end{array} & \begin{array}{c} O \\ \end{array} & \begin{array}{c} R \\ \end{array} & \begin{array}{c} O \\ \end{array} & \begin{array}{c} R \\ \end{array} & \begin{array}{c} O \\ \end{array} & \begin{array}{c} O \\ \end{array} & \begin{array}{c} R \\ \end{array} & \begin{array}{c} O \\ \end{array} & \begin{array}{c} O \\ \end{array} & \begin{array}{c} R \\ \end{array} & \begin{array}{c} O \\ \end{array} & \begin{array}{c} O \\ \end{array} & \begin{array}{c} R \\ \end{array} & \begin{array}{c} O \\ \end{array} & \begin{array}{c} O \\ \end{array} & \begin{array}{c} R \\ \end{array} & \begin{array}{c} O \\ \end{array} & \begin{array}{c} O \\ \end{array} & \begin{array}{c} R \\ \end{array} & \begin{array}{c} O \\ \end{array} &$$

Figure 5

Reaction mechanism for the formation of Kolbe products, non-Kolbe products, esters, and deep oxidation products. Figure adapted with permission from Reference 67.

simultaneous decarboxylation. This set of reactions leads to the formation of an alkyl radical and CO₂. The alkyl radical can then undergo Kolbe electrolysis through dimerization of two radicals into a longer-chain alkane, or disproportionation to a short alkane and a short alkene. Alternatively, the alkyl radical can form non-Kolbe products by undergoing further oxidation to form a carbocation, which, following deprotonation, can form an alkene (Equations 7 and 8) or react with water to form an alcohol via the Hofer–Moest reaction:

$$C_3H_6O_2 \rightarrow C_2H_4 + CO_2 + H_2$$
, $\Delta Grxn = -35 \text{ kJ/mol } C_2H_4$.

$$C_4H_8O_2 \rightarrow C_3H_6 + CO_2 + H_2$$
, $\Delta Grxn = -49 \text{ kJ/mol } C_3H_6$.

The alcohols can further react with a carboxylic acid to produce the esterification product, or they can be further oxidized to deep oxidation products such as ketones, aldehydes, or carboxylic acids (67). This mechanism applies to a broad range of carboxylic acids substituted with different functional groups and varying chain lengths. The non-Kolbe products of aliphatic acids have one fewer carbon than the starting molecule due to decarboxylation at the beginning of the mechanism (e.g., propionic acid yields ethylene, and butyric acid yields propylene).

The product distribution in (non-)Kolbe electrolysis is heavily influenced by the electrode, electrolyte, and substrate structure. Platinum is the standard working electrode for Kolbe dimerization and has a high resistance to electrochemical deactivation (61). In addition, dimerization occurs only at high current densities, such that the electrode surface is sufficiently covered by the carboxylate (68). Recent modeling studies have shown that the sluggish deprotonation of the acid on Pt oxide under aqueous conditions results in high overpotentials for Kolbe products (69). In contrast, non-Kolbe electrolysis and Hofer–Moest reactions are promoted at lower current densities due to the formation of carbenium ions (70). For non-Kolbe reactions, the most common working electrode is carbon, which is more likely to be deactivated at higher anodic potentials due to decomposition (61). Pereira et al. (71) accomplished one prominent demonstration of the synthesis of ethylene via non-Kolbe electrolysis, employing the electro-decarboxylation of a fermentation broth, which contained propionic acid, using graphite as the working electrode at room temperature. In their patent, the authors also demonstrated the non-Kolbe conversion of butyric acid into propionic acid using similar operating conditions, which emphasizes the analog reaction mechanisms of (non-)Kolbe electrolysis for substrates of different chain lengths. Several



studies have focused on the influence of the electrolyte composition on the product distribution. Methanol has been found to be the most appropriate solvent for non-Kolbe electrolysis, and acidic pH values have been found to promote the formation of carbocations (72, 73). One of main challenges with electro-decarboxylation of organic acids is that CO₂ is formed as a coproduct, lowering the decarbonization potential unless this side product is captured and mitigated. Levy et al. (74) proposed using H₂ (produced at the cathodic side) in fuel cells to recover part of the energy consumed in the Kolbe electrolysis.

ELECTROCHEMICAL AROMATICS PRODUCTION

Benzene, toluene, and xylene (BTX) together form one of the most important aromatic building blocks of the chemical industry. BTX is produced predominantly via the catalytic reforming of naphtha or hydrocarbon steam cracking (75, 76). Below, we describe alternative pathways to produce aromatics through electrochemical approaches.

Methane to Benzene

Due to the growth in natural gas production (77), the conversion of light alkanes into BTX has become increasingly desirable. An attractive catalytic route to produce aromatics is through nonoxidative methane dehydroaromatization (MDA) (Equation 9), which enables direct valorization of natural gas:

$$6CH_4 \rightarrow C_6H_6 + 9H_2$$
, $\Delta G_{rxn} = 425 \text{ kJ/mol } C_2H_4$.

The highly endothermic nature of the synthesis of benzene via MDA demands high temperatures to achieve significant benzene yields (78). Recent simulation results revealed that the maximum thermodynamically allowed conversion of methane toward benzene at 1,000°C is approximately 50% and that coke is the preferred product at this temperature (78). The challenge of achieving high conversions underscores the need for selective catalysts that are stable at operating temperatures and guarantee high yields to aromatics. To that end, MDA is performed predominantly using molybdenum nanoclusters dispersed in ZSM-5 (shape-selective zeolite) as the catalyst, which can produce high benzene selectivity at 600-800°C (79).

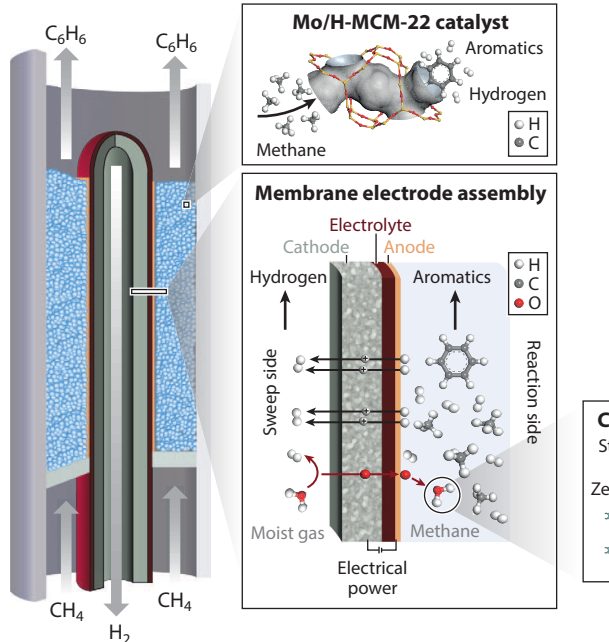
The MDA reaction faces two crucial obstacles for the reasons discussed above: (a) The reaction is limited by its thermodynamic equilibrium, which is achieved at small methane conversion, and (b) the formation of polyaromatic-type coke on the zeolite surface leads to catalyst deactivation (80, 81). Morejudo et al. (82) successfully tackled these challenges by implementing MDA in an electrocatalytic membrane reaction that used a mixed proton and oxygen ion-conducting SOEC for high and sustained aromatic yields (Figure 6). The membrane consisted of a dense BaZr_{0.7}Ce_{0.2}Y_{0.1}O_{2.9} (BZCY72) electrolyte film, which can conduct oxide ions at temperatures above 700°C. Extraction of H₂ in situ led to a shift in the equilibrium in favor of aromatics formation, thus increasing the conversion of methane beyond what is dictated by the thermodynamic equilibrium. Simultaneously, oxide ions were injected along the reactor length (proportional to H₂ extraction), improving the catalyst stability by reacting with coke to form CO. This electrochemical process resulted in a carbon efficiency exceeding 80%, similar to the Fischer-Tropsch process (82).

Biomass to Benzene, Toluene, and Xylene

An alternative electrochemical production route for aromatics is via the use of biomass feedstocks. The main components of biomass are three polymers: cellulose (30-40 wt%), hemicellulose (20-30 wt%), and lignin (10-25 wt%) (83). Cellulose and hemicellulose are commonly isolated and

Mathison et al. 9.10





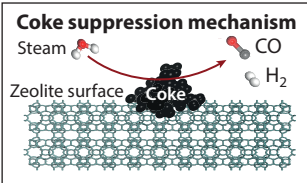


Figure 6

Catalytic membrane reactor for intensification of the methane dehydroaromatization process. The reactor is driven by a tailored co-ionic membrane that enables fast and accurate extraction of H_2 and injection of oxygen species for effective coke suppression. CH_4 is converted to benzene and hydrogen via a Mo/zeolite catalyst. Figure adapted with permission from Reference 82.

treated through established methods such as gasification for syngas or fermentation for cellulosic ethanol (84). Lignin is the most energy- and carbon-rich component of biomass and is the largest source of renewable aromatic compounds (85). Nevertheless, due to its complex chemical structure and resistance to degradation, lignin is usually burned for waste heat generation without deriving additional value (86). To valorize lignin, it needs to be depolymerized into smaller molecules for fuel or chemical production. Depolymerization can be carried out via homogeneous and heterogeneous catalytic routes, often requiring operating temperatures above 100°C (87). Alternatively, electrochemical lignin conversion and upgrading to high-value chemicals have been explored and summarized thoroughly in recent reviews (84, 88, 89). Lignin is a complex mixture of aromatic polymers produced from the oxidative coupling of three main 4-hydroxyphenylpropanoid monolignols, commonly referred to as p-hydroxyphenyl (H), guaiacyl (G), and syringyl (S) units (90). Studies have found that monolignol precursors polymerize at the β or α position of the side chain to form linkages such as β -O-4, α -O-4, and β -5, as shown in **Figure 7** (91). The most common linkage is β-O-4, which, along with other ethers, represents two-thirds of lignin linkages, the remainder of which are made up of C-C bonded monolignols (85). Previous studies have focused on the selective electrochemical cleavage of dimers and oligomers as model compounds. An early study by Mahdavi et al. (92) optimized the degradation of α-O-4 linkages through electrocatalytic hydrogenation using a Raney[®]-nickel electrode in aqueous ethanol, obtaining current efficiencies up to 80% and paving the way for more studies on hydrogenolysis of C-O linkages. Wu et al. (93) studied the cleavage of β -O-4, α -O-4, and 4-O-5 model compounds and showed that the addition of sodium borohydride promotes conversion toward aromatic monomers, resulting in a yield of



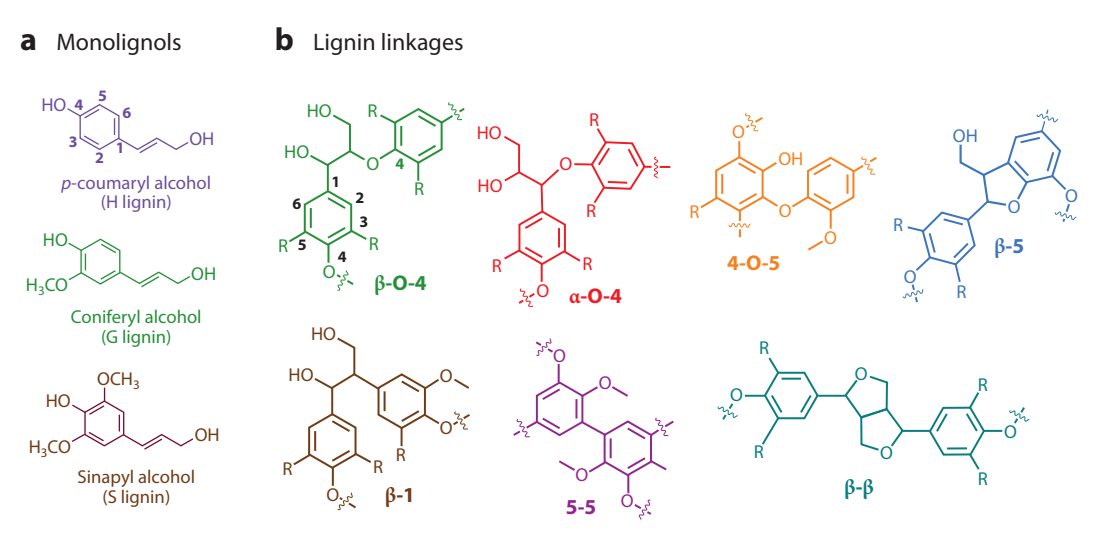


Figure 7

(a) Three main 4-hydroxyphenylpropanoid monolignols. (b) Common lignin linkages. Figure adapted with permission from Reference 84; copyright 2020 John Wiley and Sons.

more than 90% for benzene and toluene. More recently, Lan et al. (94) demonstrated the electrocatalytic degradation of cornstalk lignin in basic aqueous liquor, using a current density of 30 mA cm⁻² for 10 h and producing high-value chemicals such as toluene and ortho- and meta-xylene (36.1, 14.4, and 11.7 g/kg lignin). Although literature results show that electrochemically breaking ether bonds in dimeric models of lignin is feasible, lignin's complex and irregular nature makes its degradation into aromatic monomers a challenging task. To circumvent these barriers, further developments are needed to address the low solubility of lignin in electrolytes, identify alternative oxidation routes for its cleavage, and separate the desired product from the many products expected from electrochemical depolymerization.

ELECTROCHEMICAL PRODUCTION OF OLEFIN OXIDATION DERIVATIVES

Ethylene and propylene can be partially oxidized to produce high-value chemicals such as epoxides, alcohols, aldehydes, and acids. These important chemical commodities are currently produced via thermochemical routes, but emerging electrochemical pathways can enable their direct electrification.

Ethylene Oxidation Products

The most important product of ethylene oxidation is ethylene oxide, which is a precursor to ethylene glycol. Ethylene oxide is produced primarily by ethylene thermal epoxidation on silver catalysts (95), a process that is carried out at temperatures above 200°C and leads to a selectivity of up to 90% (96). The main competing reaction in this process is the overoxidation of ethylene to CO₂. Alternatively, ethylene can be oxidized electrochemically to produce ethylene oxide under ambient conditions (Equation 10):

$$C_2H_4 + H_2O \rightarrow CH_2CH_2O + H_2, \quad \Delta G_{rxn} = 117 \text{ kJ/mol } CH_2CH_2O \text{ (ethyleneoxide)}. \quad 10.$$

9.12 Mathison et al.



Early studies on ethylene electrochemical oxidation showed CO₂ as the main product on Pt, Ir, and Rh, whereas aldehydes were predominant by-products on Au and Pd (97). An approach to increase the epoxide selectivity is to use halide ions as redox mediators. These ions can be electrochemically oxidized to halogens, which then react with alkenes to form chlorohydrins that can further undergo an intramolecular reaction under alkaline conditions to generate epoxides. This indirect route has been explored using RuO₂ and Ru_{0.8}Co_{0.2}O₂ electrodes, where a gradual increase of chloride ion concentration inhibited CO2 formation and enabled ethylene oxide production (98). Supported by density functional theory calculations, it is hypothesized that Cl can act as a surface blocking agent that inhibits the olefin overoxidation pathway. A more recent study employed nanostructured Pd as the anode for ethylene oxidation with chloride as a redox mediator (99). The large surface area of these nanostructured Pd electrodes led to an increase in electrode-electrolyte interface, resulting in remarkably high current densities of up to 1 A cm⁻², FE up to 71% toward ethylene oxide, and stable operation over > 100 h. This pathway to ethylene oxide was integrated with CO₂ electrolyzers, whereby CO₂ is initially reduced to ethylene and the product mixture is fed directly to the anolyte of an ethylene oxidation reactor without further purification (100). The integrated CO₂-to-ethylene oxide system resulted in a 45% FE toward ethylene oxide at 300 mA cm⁻². Further optimization, aided by multiscale simulations of these integrated processes, is required to achieve a commercially viable process, but these early demonstrations present a promising path for industrial electrochemical production of ethylene oxide. An alternative method to electrochemical epoxidation of alkenes is to use water as the oxygen atom source (101). In this approach, manganese oxide nanoparticles were deposited on carbon anodes and were responsible for the epoxidation of cyclooctene, as a model alkene, with >30% FE. This demonstration provides a path to direct olefin epoxidation without the use of redox mediators, further simplifying the implementation of electrochemical manufacturing methods.

Approximately 60% of ethylene oxide production is hydrolyzed into ethylene glycol, which is then used in the production of antifreeze and polyester fibers (102). This hydrolysis reaction does not involve an electron transfer step; thus, electrifying it via electrochemistry is not feasible (103, 104). Alternatively, ethylene glycol may be produced directly from ethylene following a one-step electrochemical oxidation in aqueous media (Equation 11):

$$C_2H_4 + 2H_2O \rightarrow HOCH_2CH_2OH + H_2,$$

 $\Delta G_{rxn} = 98 \text{ kJ/mol HOCH}_2CH_2OH \text{ (ethyleneglycol)}.$ 11.

Computational studies suggest that an Au-doped Pd electrocatalyst would aid in the transfer of OH to *C₂H₄OH to form ethylene glycol at the electrocatalyst surface (105). Experimental results of such a process showed an 80% FE at 5.7 mA cm⁻² for 100 h, which is a favorable starting point for the development of a high-performing ethylene glycol electrosynthesis process.

Propylene Oxidation Products

Propylene electrooxidation follows a similar reaction pathway to ethylene due to the common vinyl group. Oxidation of the double bond in propylene leads to propylene oxide, which in the presence of water hydrolyzes to propylene glycol (Equations 12 and 13):

$$C_3H_6 + H_2O \rightarrow CH_2CHOCH_3 + H_2, \ \Delta G_{rxn} = 124 \ kJ/mol \ CH_2CHOCH_3 \ (propyleneoxide).$$
 12.

$$C_3H_6 + 2H_2O \rightarrow CH_2OHCHOHCH_3 + H_2,$$

 $\Delta G_{rxn} = 110 \text{ kJ/mol CH}_2OHCHOHCH_3 \text{ (propyleneglycol)}.$ 13.



In addition, propylene can undergo oxidation on the carbon at the allylic position, leading to allyl alcohol (Equation 14), acrolein (Equation 15), and acrylic acid (Equation 16):

$$C_3H_6+H_2O\rightarrow CH_2CHCH_2OH+H_2,\ \Delta G_{rxn}=100\ kJ/mol\ CH_2CHCH_2OH\ (allylalcohol).$$
 14.

$$C_3H_6 + H_2O \rightarrow CH_2CHCHO + 2H_2$$
, $\Delta G_{rxn} = 138 \text{ kJ/mol CH}_2CHCHO$ (acrolein). 15.

$$C_3H_6 + 2H_2O \rightarrow CH_2CHCOOH + 3H_2, \ \Delta G_{rxn} = 209 \ kJ/mol \ CH_2CHCOOH (acrylicacid).$$

Current thermochemical methods to produce propylene oxide involve the indirect Cl₂-or organic peroxide-mediated oxidation of propylene (106). Thermochemical production of acrolein or acrylic acid relies on high-temperature/high-pressure direct air oxidation over cuprous oxide and cobalt molybdate catalysts, respectively (107). These oxidation processes are difficult to control, have a relatively low yield, and often result in overoxidation of propylene to CO₂ (108). Also, the indirect methods require stoichiometric oxidants that add to the cost, energy demand, and complexity of the process (3).

In an early study, Holbrook & Wise (109) reported the formation of propylene oxide on anodic Ag and Au surfaces at small current densities (below 0.01 mA cm⁻²). Following publications showed that the most favorable results for propylene oxidation are obtained using Pd electrodes in acidic environments (110, 111). More recently, Winiwarter et al. (112, 113) demonstrated that the selectivity toward each oxidation center is highly dependent on the surface coverage of the species in the Pd electrocatalyst, as shown in Figure 8. With high surface coverage at low potentials (e.g., <1 V), binding of the allylic position is geometrically preferred, leading to the oxidation of this center. On the other hand, the production of propylene oxide requires the vinylic adsorption of

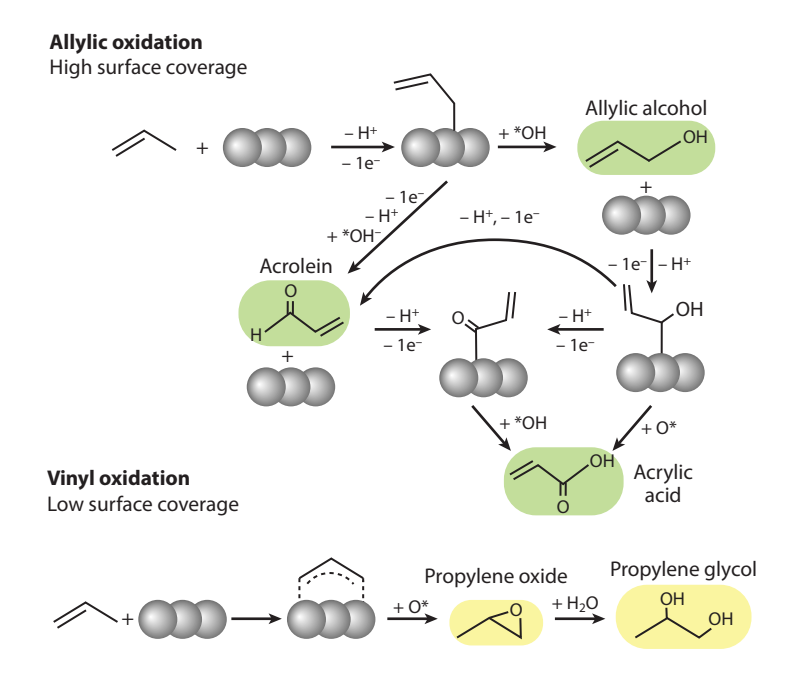


Figure 8

Proposed mechanism of propylene electrocatalytic oxidation. The product distribution is dictated by the coverage regime. Figure adapted with permission from Reference 112.

Mathison et al. 9.14



propylene, which forces the molecule to lie flat in the catalyst surface. Due to steric effects, this is preferred only when the surface coverage of organic species is low at high potentials (e.g., >1 V). Subsequently, propylene oxide can homogeneously react with water to produce propylene glycol. The mechanistic findings of these reports are crucial for identifying the key reaction steps that can lead to selectivity control. A follow-up study implemented density functional theory and microkinetic modeling to understand the direct epoxidation of propylene using molecular oxygen from water splitting (114). Results from this study provide a guide for stable design of weak-biding catalysts (e.g., Au, PbO₂, PdO₂) as anode materials for propylene oxide synthesis.

ELECTROCHEMICAL METHANOL PRODUCTION

Methanol is an important energy vector with high energy density (15.6 MJ L⁻¹) that can be used as a green fuel (115). In addition, methanol also serves as a basic feedstock chemical for plastics production. Most industrial methanol production comes from syngas, which is produced through methane steam reforming using nickel-based catalysts at temperatures of 800-1,000°C and pressures of 290-580 psi (116). By contrast, electrochemical methanol production methods can be implemented at temperatures <300°C and even at ambient conditions.

CO₂ and CO to Methanol

As discussed in previous sections, electrochemical CO₂RR results in a mixture of products whose distribution depends on the electrocatalyst and medium used (117). Among those products, methanol presents one of the largest economic and environmental opportunities. The most recent advances in electrochemical CO₂RR to methanol (Equation 17) are summarized in this section and discussed in depth in recent reviews (118-121):

$$CO_2 + 2H_2O \rightarrow CH_3OH + 1^1/2O_2$$
, $\Delta G_{rxn} = 702 \text{ kJ/mol CH}_3OH$. 17.

The reduction of CO₂ toward methanol consists of 6 electron transfer steps and faces strong competition from HER (118), and thus requires highly selective electrocatalysts capable of suppressing HER and promoting methanol formation. Two possible mechanisms have been proposed for CO₂RR toward methanol, which are distinguished by having either CO (122) or formate (HCOO⁻) (123) as the main reaction intermediate.

The first demonstration of methanol synthesis from CO₂ electroreduction is attributed to Canfield & Frese (124), using a photoelectrochemical method that relied on semiconductors n- and p-GaAs and p-InP as electrodes under illumination. Since then, researchers have explored the implementation of several electrocatalysts ranging from metal alloys, metal oxides, and organometallic and inorganic complexes to pyridine and metal-organic frameworks. Metal alloys can improve CO₂RR reaction kinetics and selectivity by adjusting the binding energy of active intermediates (125). A Pd₈₃Cu₁₇ aerogel electrocatalyst was developed and exhibited a FE of 80% toward methanol at a current density up to 31.8 mA cm⁻² under [Bmim]BF₄-water mixture electrolyte; the efficient performance was attributed to the synergistic contributions from Pd and Cu (126). Zhang et al. (127) employed Cu overlayers on Pd nanocrystals, resulting in a distribution of products that depended on Cu coverage in the catalyst, achieving the largest FE toward methanol (19.5%) at 0.8 monolayers of Cu. Some metal oxides also exhibit high selectivity toward methanol, as Periasamy et al. (128) demonstrated, achieving a methanol FE of 93% using cuprous oxide/polypyrrole electrocatalysts at low current densities (<0.25 mA cm⁻²). To improve current densities, Albo et al. (129) demonstrated a continuous electrochemical cell with Cu₂O-based GDE in 0.5 M KHCO₃ aqueous electrolyte. The study showed a maximum of 42.3% FE at 10 mA cm⁻²; however, selectivity dropped drastically as the current was increased. Several other metal oxides



have been shown to selectively reduce CO_2 toward methanol, including in a prominent study using Pd/SnO_2 (130). A recent demonstration using $Cu_{1.63}Se(1/3)$ nanocatalysts achieved a 77.6% FE toward methanol at 41.5 mA cm⁻² (131). An alternative strategy is to use pyridine-doped palladium electrocatalysts, which exhibited a remarkable current density of 52 mA cm⁻² and methanol FE of 35% (132). In this class of catalysts, metallic Pd acted as the heterogeneous support, and a pyridine served as an active site for CO_2 reduction.

In addition to the employed electrocatalyst, the reaction medium and supporting electrolytes have a considerable impact on the selectivity and efficiency of CO₂RR. The rate of CO₂RR toward methanol at low overpotentials increases with the surface charge of the supporting cation, which is attributed to adsorption in the electrode surface and polarization of intermediate radicals (133). The choice of the anion influences the local pH, which translates into proton availability and hence affects the reaction kinetics for pathways leading to methanol production and competing HER.

The CO₂RR toward CO has been reported extensively, in particular with Ag-based electrodes (134). Given that CO has been identified as a key intermediate for CO₂ electroreduction to methanol, designing a two-step process for methanol production could result in enhanced performance (Equation 18):

$$CO + 2H_2O \rightarrow CH_3OH + O_2$$
, $\Delta G_{rxn} = 445 \text{ kJ/mol CH}_3OH$. 18.

Wu et al. (135) recently explored this tandem concept, using a single layer of Cophthalocyanine (Co-Pc) on carbon nanotubes (CNT) for both reaction steps and achieving a methanol FE >40% at 10 mA cm⁻².

Methane to Methanol

An alternative route for methanol production is through direct methane electrooxidation (Equations 19 and 20):

$$CH_4 + \frac{1}{2}O_2 \rightarrow CH_3OH$$
, $\Delta G_{rxn} = -116 \text{ kJ/mol CH}_3OH$. 19.

$$CH_4 + H_2O \rightarrow CH_3OH + H_2$$
, $\Delta G_{rxn} = 121 \text{ kJ/mol CH}_3OH$. 20.

In addition to the abundance and affordability of natural gas, methanol production from methane requires substantially less energy than if it were produced from CO₂. These advantages have motivated researchers to investigate electrochemical methane oxidation to methanol at low to mild temperatures (<300°C) (136–138). Due to the high stability of methane (i.e., 439 kJ mol⁻¹ are needed to break one C-H bond) (139), C-H activation plays a critical role in the performance of this reaction. Additionally, methanol has a significant risk of being oxidized to formaldehyde, formic acid, or CO₂ if anodic conditions are not carefully controlled. These challenges accentuate the need for a catalyst and reaction conditions with superior selectivity toward methanol. For instance, operation at higher temperatures facilitates methane activation but endangers full oxidation of methanol (140). The reaction conditions at which methanol is selectively produced have been investigated under different electrocatalysts and cell configurations, and key findings are summarized below.

The materials used as anodes for direct methane activation are divided into metals, metal oxides/promoted oxygenated surfaces, and ZrO₂ composites (137). Theoretical calculations have shown that among metals, Pt exhibits the highest rates of methane activation (141). As a result, most demonstrations using metallic electrocatalysts implement Pt as the anode (137), but the adsorption rates of methane on Pt surfaces are slower than the oxidation rates to CO₂, leading

9.16 Mathison et al.



to low methanol selectivity (141, 142). Metal oxides are also a promising class of electrocatalysts for methane partial oxidation. Most of the employed metal oxides contain transition metal compounds (e.g., Ni, V, Ru, Ir), which often are used as catalysts in thermal reactions (143). A recent modeling study identified promising metal oxide candidates for methane-to-methanol conversion and concluded that methane is thermochemically activated and that mild temperatures (>100°C) can facilitate C-H activation (144). A notable demonstration of methane-to-methanol conversion in metal oxide electrocatalysts implemented Rh single atoms dispersed in a NiO and V_2O_5 nanocomposite and achieved a FE of 91% toward methanol at 25 mA cm⁻² and 100°C (145). Lastly, composites made of a ZrO₂ matrix with metal oxide nanoparticles are emerging electrocatalysts for methane activation (146). Theoretical calculations suggest that these composites improve performance because the methane activation barrier is decreased by the high-speed electron transfer network between ZrO₂ and the metal oxide (147).

Electrochemical oxidation of methane in aqueous electrolytes has been explored recently as well, despite some substantial limitations. The low solubility of methane in water limits the achievable current densities, and a narrow window of potentials can convert methane into methanol without competing with the oxygen evolution reaction. One way to address these issues is to electrochemically generate redox mediators that can indirectly oxidize methane. For example, Pt^{II} mediators can be electrochemically generated from Pt^{IV} and partially oxidize methane to methanol. A recent study that implemented this Pt^{II}/Pt^{IV} electrochemical cycle demonstrated a selectivity of 70% toward methanol (148). Alternative methods to aqueous electrolytes involve the use of ceramic membranes that can operate at higher temperatures and thus favor methane activation. A frequently used ceramic material for methane oxidation is $Sn_{0.9}In_{0.1}P_2O_7$ due to its high proton conductivity (>10⁻¹ S cm⁻¹) at moderate temperatures (100–350°C). Demonstrations using this ceramic (149, 150) exhibit a sharp decrease in methanol selectivity as temperature is increased due to overoxidation, emphasizing the need for a solid electrolyte with sufficiently high conductivities at lower temperatures.

OUTLOOK AND PERSPECTIVE

This review summarized approaches to electrochemical manufacturing of major organic chemical commodities. Most of the studies highlighted above involved laboratory-scale demonstration of electro-organic reactions, but achieving large-scale production remains a challenge. Scaling the advances in electrochemical catalysis and reaction engineering reviewed in this article will require that reactions operate stably for long periods of time at high current density, selectivity, and energy conversion efficiency. Multiple research strategies are required to achieve these reaction performance metrics, which include

- Current density: discovering and engineering highly active electrocatalysts, achieving stable electrode structures with high electrochemical surface area, and controlling mass transfer processes to achieve rapid transport of reactants and products to and from reaction sites.
- Selectivity: developing a mechanistic understanding of each transformation, engineering multicomponent electrocatalysts with control over multiple surface intermediates, understanding and controlling microenvironments at electrocatalysts/electrolyte interfaces, and exploiting nonequilibrium electrocatalytic processes via control of dynamic electrochemical operation.
- Energy efficiency: minimizing kinetic losses via electrocatalyst development and control of electrocatalyst–electrolyte interfaces, mitigating ohmic losses via the implementation of highly conductive liquid or solid electrolytes, and managing transport processes to avoid concentration overpotential losses.



■ Stability: establishing reliable, accelerated stability testing protocols and developing protection strategies for electrocatalysts and ion-conducting membranes.

The fundamental science advances highlighted in this review provide some initial insights into mechanisms to control selectivity and reactivity in electrochemical reactions relevant to chemical manufacturing. These insights are important to achieve high performance metrics for electroorganic reactions, allowing the chemical engineering community to start to develop scale-up and design guidelines for practical electrochemical reactors. This will in turn enable the deployment of electrochemical manufacturing processes at the scales required for producing bulk chemical commodities, helping to electrify and decarbonize the chemical industry.

DISCLOSURE STATEMENT

M.A.M. is a cofounder of and has financial interests in Sunthetics Inc., a company operating on the sustainable chemical manufacturing space. The authors are not aware of any affiliations, memberships, funding, or financial holdings that might be perceived as affecting the objectivity of this review.

ACKNOWLEDGMENTS

The authors acknowledge the financial support provided by the National Science Foundation (NSF), the Sloan Foundation, and New York University Tandon School of Engineering. This material is based upon work supported by the NSF under grant 1943972 and the Sloan Foundation under grant 201-16807.

LITERATURE CITED

- US Dep. Energy. 2018. Manufacturing energy and carbon footprints report, 2018. Rep., Adv. Manuf. Off., US Dep. Energy., Washington, DC. https://www.energy.gov/sites/default/files/2021-12/2018_mecs_chemicals_energy_carbon_footprint_0.pdf
- Mallapragada D, Dvorkin Y, Modestino M, Esposito D, Smith W, et al. 2022. Decarbonization of the chemical industry through electrification: barriers and opportunities. ChemRxiv. https://doi.org/ 10.26434/chemrxiv-2022-00gls
- Biddinger EJ, Modestino MA. 2020. Electro-organic syntheses for green chemical manufacturing. Electrochem. Soc. Interface 29:43–47
- Schiffer ZJ, Manthiram K. 2017. Electrification and decarbonization of the chemical industry. Joule 1:10–14
- De Luna P, Hahn C, Higgins D, Jaffer SA, Jaramillo TF, Sargent EH. 2019. What would it take for renewably powered electrosynthesis to displace petrochemical processes? Science 364:eaav3506
- Blanco DE, Modestino MA. 2019. Organic electrosynthesis for sustainable chemical manufacturing. Trends Chem. 1:8–10
- Botte GG. 2014. Electrochemical manufacturing in the chemical industry. Electrochem. Soc. Interface 23:49–55
- 8. US Dep. Energy. 2015. Bandwidth study on energy use and potential energy saving opportunities in U.S. chemical manufacturing. Rep., Energy Effic. Renew. Energy, US Dep. Energy, Washington, DC. https://www.energy.gov/sites/prod/files/2015/08/f26/chemical_bandwidth_report.pdf
- Amghizar I, Dedeyne JN, Brown DJ, Marin GB, Van Geem KM. 2020. Sustainable innovations in steam cracking: CO₂ neutral olefin production. *React. Chem. Eng.* 5:239–57
- Ghanta M, Fahey D, Subramaniam B. 2013. Environmental impacts of ethylene production from diverse feedstocks and energy sources. Appl. Petrochem. Res. 4:167–79
- Nitopi S, Bertheussen E, Scott SB, Liu X, Engstfeld AK, et al. 2019. Progress and perspectives of electrochemical CO₂ reduction on copper in aqueous electrolyte. *Chem. Rev.* 119:7610–72

9.18 Mathison et al.



 Zhang Z, Bian L, Tian H, Liu Y, Bando Y, et al. 2022. Tailoring the surface and interface structures of copper-based catalysts for electrochemical reduction of CO₂ to ethylene and ethanol. Small 18:e2107450

12:25

- Pappijn CAR, Ruitenbeek M, Reyniers M-F, Van Geem KM. 2020. Challenges and opportunities of carbon capture and utilization: electrochemical conversion of CO₂ to ethylene. Front. Energy Res. 8:557466
- Xia R, Overa S, Jiao F. 2022. Emerging electrochemical processes to decarbonize the chemical industry. 7ACS Au 2:1054–70
- Hori Y, Kikuchi K, Murata A, Suzuki S. 1986. Production of methane and ethylene in electrochemical reduction of carbon dioxide at copper electrode in aqueous hydrogenearbonate solution. Chem. Lett. 15:897–98
- Hori Y, Murata A, Takahashi R, Suzuki S. 1988. Enhanced formation of ethylene and alcohols at ambient temperature and pressure in electrochemical reduction of carbon dioxide at a copper electrode. J. Chem. Soc. Chem. Commun. 1988:17–19
- Roberts FS, Kuhl KP, Nilsson A. 2015. High selectivity for ethylene from carbon dioxide reduction over copper nanocube electrocatalysts. Angew. Chem. Int. Ed. 54:5179

 –82
- Reller C, Krause R, Volkova E, Schmid B, Neubauer S, et al. 2017. Selective electroreduction of CO₂ toward ethylene on nano dendritic copper catalysts at high current density. Adv. Energy Mater. 7:1602114
- Dinh C-T, Burdyny T, Kibria MG, Seifitokaldani A, Gabardo CM, et al. 2018. CO₂ electroreduction to ethylene via hydroxide-mediated copper catalysis at an abrupt interface. Science 360:783–87
- Bagger A, Ju W, Varela AS, Strasser P, Rossmeisl J. 2017. Electrochemical CO₂ reduction: a classification problem. ChemPhysChem 18:3266–73
- Kortlever R, Shen J, Schouten KJ, Calle-Vallejo F, Koper MTM. 2015. Catalysts and reaction pathways for the electrochemical reduction of carbon dioxide. J. Phys. Chem. Lett. 6:4073–82
- Hori Y, Murata A, Ito S-y, Yoshinami Y, Koga O. 1989. Nickel and iron modified copper electrode for electroreduction of CO₂ by in-situ electrodeposition. Chem. Lett. 18:1567–70
- Kim D, Resasco J, Yu Y, Asiri AM, Yang P. 2014. Synergistic geometric and electronic effects for electrochemical reduction of carbon dioxide using gold-copper bimetallic nanoparticles. *Nat. Commun.* 5:4948
- 24. Ye W, Guo X, Ma T. 2021. A review on electrochemical synthesized copper-based catalysts for electrochemical reduction of CO₂ to C₂₊ products. *Chem. Eng. J.* 414:128825
- Akira M, Yoshio H. 1991. Product selectivity affected by cationic species in electrochemical reduction of CO₂ and CO at a Cu electrode. Bull. Chem. Soc. Jpn. 64:123–27
- Hori Y, Takahashi R, Yoshinami Y, Murata A. 1997. Electrochemical reduction of CO at a copper electrode. 7. Phys. Chem. B 101:7075–81
- Hori Y, Murata A, Takahashi R, Suzuki S. 1987. Electroreduction of carbon monoxide to methane and ethylene at a copper electrode in aqueous solutions at ambient temperature and pressure. J. Am. Chem. Soc. 109:5022–23
- Chen X, Chen J, Alghoraibi NM, Henckel DA, Zhang R, et al. 2020. Electrochemical CO₂-to-ethylene conversion on polyamine-incorporated Cu electrodes. Nat. Catal. 4:20–27
- 29. Li F, Thevenon A, Rosas-Hernández A, Wang Z, Li Y, et al. 2020. Molecular tuning of CO₂-to-ethylene conversion. *Nature* 577:509–13
- Kim C, Bui JC, Luo X, Cooper JK, Kusoglu A, et al. 2021. Tailored catalyst microenvironments for CO₂ electroreduction to multicarbon products on copper using bilayer ionomer coatings. *Nat. Energy* 6:1026–34
- Kim C, Weng L-C, Bell AT. 2020. Impact of pulsed electrochemical reduction of CO₂ on the formation of C₂₊ products over Cu. ACS Catal. 10:12403–13
- De Gregorio GL, Burdyny T, Loiudice A, Iyengar P, Smith WA, Buonsanti R. 2020. Facet-dependent selectivity of Cu catalysts in electrochemical CO₂ reduction at commercially viable current densities. ACS Catal. 10:4854–62
- Lum Y, Yue B, Lobaccaro P, Bell AT, Ager JW. 2017. Optimizing C–C coupling on oxide-derived copper catalysts for electrochemical CO₂ reduction. J. Phys. Chem. C 121:14191–203
- Hashiba H, Yotsuhashi S, Deguchi M, Yamada Y. 2016. Systematic analysis of electrochemical CO₂ reduction with various reaction parameters using combinatorial reactors. ACS Comb. Sci. 18:203–8





- Burdyny T, Smith WA. 2019. CO₂ reduction on gas-diffusion electrodes and why catalytic performance must be assessed at commercially-relevant conditions. *Energy Environ. Sci.* 12:1442–53
- 36. García de Arquer FP, Dinh C-T, Ozden A, Wicks J, McCallum C, et al. 2020. CO₂ electrolysis to multicarbon products at activities greater than 1 A cm⁻². Science 367:661–66
- Jouny M, Hutchings GS, Jiao F. 2019. Carbon monoxide electroreduction as an emerging platform for carbon utilization. Nat. Catal. 2:1062–70
- 38. Kumar B, Llorente M, Froehlich J, Dang T, Sathrum A, Kubiak CP. 2012. Photochemical and photoelectrochemical reduction of CO₂. *Annu. Rev. Phys. Chem.* 63:541–69
- Vasileff A, Zhi X, Xu C, Ge L, Jiao Y, et al. 2019. Selectivity control for electrochemical CO₂ reduction by charge redistribution on the surface of copper alloys. ACS Catal. 9:9411–17
- Wang L, Nitopi SA, Bertheussen E, Orazov M, Morales-Guio CG, et al. 2018. Electrochemical carbon monoxide reduction on polycrystalline copper: effects of potential, pressure, and pH on selectivity toward multicarbon and oxygenated products. ACS Catal. 8:7445–54
- Li CW, Ciston J, Kanan MW. 2014. Electroreduction of carbon monoxide to liquid fuel on oxide-derived nanocrystalline copper. Nature 508:504–7
- Bertheussen E, Verdaguer-Casadevall A, Ravasio D, Montoya JH, Trimarco DB, et al. 2016. Acetaldehyde as an intermediate in the electroreduction of carbon monoxide to ethanol on oxide-derived copper. *Angew. Chem. Int. Ed.* 55:1450–54
- Han L, Zhou W, Xiang C. 2018. High-rate electrochemical reduction of carbon monoxide to ethylene using Cu-nanoparticle-based gas diffusion electrodes. ACS Energy Lett. 3:855–60
- Li J, Wang Z, McCallum C, Xu Y, Li F, et al. 2019. Constraining CO coverage on copper promotes high-efficiency ethylene electroproduction. *Nat. Catal.* 2:1124–31
- 45. Ozden A, Wang Y, Li F, Luo M, Sisler J, et al. 2021. Cascade CO₂ electroreduction enables efficient carbonate-free production of ethylene. *Joule* 5:706–19
- Romero Cuellar NS, Scherer C, Kaçkar B, Eisenreich W, Huber C, et al. 2020. Two-step electrochemical reduction of CO₂ towards multi-carbon products at high current densities. J. CO₂ Util. 36:263–75
- 47. Gurudayal Perone D, Malani S, Lum Y, Haussener S, Ager JW. 2019. Sequential cascade electrocatalytic conversion of carbon dioxide to C–C coupled products. ACS Appl. Energy Mater. 2:4551–59
- 48. Zhu P-X, Wang L-C, Stewart F, Ding D, Matz J, et al. 2021. Direct conversion of natural gases in solid oxide cells: a mini-review. *Electrochem. Commun.* 128:107068
- Wu W, Wang L-C, Hu H, Bian W, Gomez JY, et al. 2021. Electrochemically engineered, highly energy-efficient conversion of ethane to ethylene and hydrogen below 550°C in a protonic ceramic electrochemical cell. ACS Catal. 11:12194–202
- Zhang X, Ye L, Li H, Chen F, Xie K. 2020. Electrochemical dehydrogenation of ethane to ethylene in a solid oxide electrolyzer. ACS Catal. 10:3505–13
- Zhu C, Hou S, Hu X, Lu J, Chen F, Xie K. 2019. Electrochemical conversion of methane to ethylene in a solid oxide electrolyzer. *Nat. Commun.* 10:1173
- 52. Gunduz S, Dogu D, Deka DJ, Meyer KE, Fuller A, et al. 2019. Application of solid electrolyte cells in ion pump and electrolyzer modes to promote catalytic reactions: an overview. *Catal. Today* 323:3–13
- 53. Metcalfe IS. 1994. Stabilised-zirconia solid electrolyte membranes in catalysis. Catal. Today 20:283–93
- 54. Skinner SJ, Kilner JA. 2003. Oxygen ion conductors. Mater. Today 6:30-37
- Duan C, Huang J, Sullivan N, O'Hayre R. 2020. Proton-conducting oxides for energy conversion and storage. Appl. Phys. Rev. 7:011314
- 56. Duan C, Kee RJ, Zhu H, Karakaya C, Chen Y, et al. 2018. Highly durable, coking and sulfur tolerant, fuel-flexible protonic ceramic fuel cells. *Nature* 557:217–22
- 57. Ding D, Zhang Y, Wu W, Chen D, Liu M, He T. 2018. A novel low-thermal-budget approach for the co-production of ethylene and hydrogen via the electrochemical non-oxidative deprotonation of ethane. *Energy Environ. Sci.* 11:1710–16
- 58. Wu W, Hu H, Ding D. 2021. Low-temperature ethylene production for indirect electrification in chemical production. *Cell Rep. Phys. Sci.* 2:100405
- Lin J-Y, Shao L, Si F-Z, Liu S-B, Fu X-Z, Luo J-L. 2018. Co₂CrO₄ nanopowders as an anode catalyst for simultaneous conversion of ethane to ethylene and power in proton-conducting fuel cell reactors. J. Phys. Chem. C 122:4165-71

9.20 Mathison et al.



- 60. Zavyalova U, Holena M, Schlögl R, Baerns M. 2011. Statistical analysis of past catalytic data on oxidative methane coupling for new insights into the composition of high-performance catalysts. ChemCatChem. 3:1935-47
- 61. Holzhäuser FJ, Mensah JB, Palkovits R. 2020. (Non-)Kolbe electrolysis in biomass valorization—a discussion of potential applications. Green Chem. 22:286-301
- 62. Mortensen PM, Grunwaldt JD, Jensen PA, Knudsen KG, Jensen AD. 2011. A review of catalytic upgrading of bio-oil to engine fuels. Appl. Catal. A 407:1-19
- 63. Iglesias J, Martínez-Salazar I, Maireles-Torres P, Martin Alonso D, Mariscal R, López-Granados M. 2020. Advances in catalytic routes for the production of carboxylic acids from biomass: a step forward for sustainable polymers. Chem. Soc. Rev. 49:5704-71
- 64. Andreev VN, Grinberg VA, Dedov AG, Loktev AS, Moiseev II, Tsivadze AY. 2013. Electrocatalytic biomass conversion into petrochemicals. Review. Prot. Metals Phys. Chem. Surf. 49:32-39
- 65. Wiebe A, Gieshoff T, Mohle S, Rodrigo E, Zirbes M, Waldvogel SR. 2018. Electrifying organic synthesis. Angew. Chem. Int. Ed. 57:5594-619
- Qiu Y, Lopez-Ruiz JA, Sanyal U, Andrews E, Gutiérrez OY, Holladay JD. 2020. Anodic electrocatalytic conversion of carboxylic acids on thin films of RuO2, IrO2, and Pt. Appl. Catal. B 277:119277
- Qiu Y, Lopez-Ruiz JA, Zhu G, Engelhard MH, Gutiérrez OY, Holladay JD. 2022. Electrocatalytic decarboxylation of carboxylic acids over RuO2 and Pt nanoparticles. Appl. Catal. B 305:121060
- Kapałka A, Lanova B, Baltruschat H, Fóti G, Comninellis C. 2008. DEMS study of the acetic acid oxidation on boron-doped diamond eelectrode. J. Electrochem. Soc. 155:E96
- Liu S, Govindarajan N, Prats H, Chan K. 2022. Understanding the reaction mechanism of Kolbe electrolysis on Pt anodes. Chem. Catal. 2:1100-13
- Schäfer H-I. 1990. Recent contributions of Kolbe electrolysis to organic synthesis. In *Electrochemistry* IV: Topics in Current Chemistry, ed. E Steckhan, pp. 91-151. Berlin, Heidelberg: Springer
- 71. Pereira GAG, Perez JR, Carazzolle MF, de Castro Morschbacker ALR, Roza L, dos Santos Andrade MH. 2013. Method for the production of olefins, an olefin, a polyolefin, and use of the polyolefin. US Patent No. 20130203953A1
- 72. Meyers J, Mensah JB, Holzhäuser FJ, Omari A, Blesken CC, et al. 2019. Electrochemical conversion of a bio-derivable hydroxy acid to a drop-in oxygenate diesel fuel. Energy Environ. Sci. 12:2406-11
- 73. Creusen G, Holzhäuser FJ, Artz J, Palkovits S, Palkovits R. 2018. Producing widespread monomers from biomass using economical carbon and ruthenium-titanium dioxide electrocatalysts. ACS Sustain. Chem. Eng. 6:17108-13
- 74. Levy P, Sanderson J, Kispert R, Wise D. 1981. Biorefining of biomass to liquid fuels and organic chemicals. Enzyme Microb. Technol. 3:207-15
- 75. Int. Energy Agency. 2006. Energy technology perspectives 2006. Rep., Int. Energy Agency, Paris. https:// www.iea.org/reports/energy-technology-perspectives-2006
- 76. Nexant Inc. 2007. Benzene/Toluene. Rep. PERP 06/07-6, Nexant Inc., London
- 77. Wu W, Gaffney A, Ding D. 2020. Electrochemical conversion of natural gas to value added chemicals. In Direct Natural Gas Conversion to Value-Added Chemicals, ed. J Hu, D Shekhawat, pp. 1-24. Boca Raton, FL: CRC Press
- 78. Kosinov N, Hensen EJM. 2020. Reactivity, selectivity, and stability of zeolite-based catalysts for methane dehydroaromatization. Adv. Mater. 32:e2002565
- 79. Gao J, Zheng Y, Jehng J-M, Tang Y, Wachs IE, Podkolzin SG. 2015. Identification of molybdenum oxide nanostructures on zeolites for natural gas conversion. Science 348:686-90
- Tempelman CHL, Hensen EJM. 2015. On the deactivation of Mo/HZSM-5 in the methane dehydroaromatization reaction. Appl. Catal. B 176-77:731-39
- 81. Vourros A, Kyriakou V, Garagounis I, Vasileiou E, Stoukides M. 2017. Chemical reactors with high temperature proton conductors as a main component: progress in the past decade. Solid State Ion. 306:76-
- 82. Morejudo SH, Zanón R, Escolástico S, Yuste-Tirados I, Malerød-Fjeld H, et al. 2016. Direct conversion of methane to aromatics in a catalytic co-ionic membrane reactor. Science 353:563-66
- 83. Biswas R, Uellendahl H, Ahring BK. 2015. Wet explosion: a universal and efficient pretreatment process for lignocellulosic biorefineries. BioEnergy Res. 8:1101-16





- 84. Garedew M, Lin F, Song B, DeWinter TM, Jackson JE, et al. 2020. Greener routes to biomass waste valorization: lignin transformation through electrocatalysis for renewable chemicals and fuels production. ChemSusChem 13:4214–37
- Zakzeski J, Bruijnincx PCA, Jongerius AL, Weckhuysen BM. 2010. The catalytic valorization of lignin for the production of renewable chemicals. *Chem. Rev.* 110:3552–99
- Gosselink RJA, de Jong E, Guran B, Abächerli A. 2004. Co-ordination network for lignin standardisation, production and applications adapted to market requirements (EUROLIGNIN). Ind. Crops. Prod. 20:121–29
- Zhang Z, Song J, Han B. 2017. Catalytic transformation of lignocellulose into chemicals and fuel products in ionic liquids. *Chem. Rev.* 117:6834–80
- 88. Garedew M, Lam CH, Petitjean L, Huang S, Song B, et al. 2021. Electrochemical upgrading of depolymerized lignin: a review of model compound studies. *Green Chem.* 23:2868–99
- Du X, Zhang H, Sullivan KP, Gogoi P, Deng Y. 2020. Electrochemical lignin conversion. ChemSusChem 13:4318–43
- Vanholme R, Demedts B, Morreel K, Ralph J, Boerjan W. 2010. Lignin biosynthesis and structure. Plant Physiol. 153:895–905
- 91. Chioccara F, Poli S, Rindone B, Pilati T, Brunow G, et al. 1993. Regio- and diastereo-selective synthesis of dimeric lignans using oxidative coupling. *Acta Chem. Scand.* 47:610–16
- 92. Mahdavi B, Lafrance A, Martel A, Lessard J, Brossard L. 1997. Electrocatalytic hydrogenolysis of lignin model dimers at Raney nickel electrodes. *J. Appl. Electrochem.* 27:605–11
- Wu WB, Huang JM. 2014. Electrochemical cleavage of aryl ethers promoted by sodium borohydride.
 Org. Chem. 79:10189–95
- 94. Lan C, Fan H, Shang Y, Shen D, Li G. 2020. Electrochemically catalyzed conversion of cornstalk lignin to aromatic compounds: an integrated process of anodic oxidation of a Pb/PbO₂ electrode and hydrogenation of a nickel cathode in sodium hydroxide solution. *Sustain. Energy Fuels* 4:1828–36
- 95. Hernández Carucci JR, Halonen V, Eränen K, Wärnå J, Ojala S, et al. 2010. Ethylene oxide formation in a microreactor: from qualitative kinetics to detailed modeling. *Ind. Eng. Chem. Res.* 49:10897–907
- Özbek MO, van Santen RA. 2013. The mechanism of ethylene epoxidation catalysis. Catal. Lett. 143:131– 41
- Dahms H, Bockris JOM. 1964. The relative electrocatalytic activity of noble metals in the oxidation of ethylene. J. Electrochem. Soc. 111:728
- Jirkovsky JS, Busch M, Ahlberg E, Panas I, Krtil P. 2011. Switching on the electrocatalytic ethene epoxidation on nanocrystalline RuO₂. *J. Am. Chem. Soc.* 133:5882–92
- 99. Leow WR, Lum Y, Ozden A, Wang Y, Nam D-H, et al. 2020. Chloride-mediated selective electrosynthesis of ethylene and propylene oxides at high current density. *Science* 368:1228–33
- Barecka MH, Ager JW, Lapkin AA. 2021. Economically viable CO₂ electroreduction embedded within ethylene oxide manufacturing. *Energy Environ. Sci.* 14:1530–43
- 101. Jin K, Maalouf JH, Lazouski N, Corbin N, Yang D, Manthiram K. 2019. Epoxidation of cyclooctene using water as the oxygen atom source at manganese oxide electrocatalysts. J. Am. Chem. Soc. 141:6413– 18
- Rebsdat S, Mayer D. 2000. Ethylene oxide. In *Ullmann's Encyclopedia of Industrial Chemistry*. Hoboken, NJ: Wiley
- Lundin A, Panas I, Ahlberg E. 2007. A mechanistic investigation of ethylene oxide hydrolysis to ethanediol. J. Phys. Chem. A 111:9087–92
- 104. Muniz Filho RCD, Alves de Sousa SA, da Silva Pereira F, Castro Ferreira MM. 2010. Theoretical study of acid-catalyzed hydrolysis of epoxides. J. Phys. Chem. A 114:5187–94
- Lum Y, Huang JE, Wang Z, Luo M, Nam D-H, et al. 2020. Tuning OH binding energy enables selective electrochemical oxidation of ethylene to ethylene glycol. Nat. Catal. 3:14–22
- Khatib SJ, Oyama ST. 2015. Direct oxidation of propylene to propylene oxide with molecular oxygen: a review. Catal. Rev. 57:306–44
- 107. Speight JG. 2019. Handbook of Petrochemical Processes. Boca Raton, FL: CRC Press

9.22 Mathison et al.



- 108. Ghanta M, Ruddy T, Fahey D, Busch D, Subramaniam B. 2012. Is the liquid-phase H₂O₂-based ethylene oxide process more economical and greener than the gas-phase O₂-based silver-catalyzed process? *Ind. Eng. Chem. Res.* 52:18–29
- 109. Holbrook L, Wise H. 1975. Electrooxidation of olefins at a silver electrode. 7. Catal. 38:294-98
- 110. Stafford GR. 1987. The electrogenerative partial oxidation of propylene. Electrochim. Acta 32:1137-43
- 111. Otsuka K, Shimizu Y, Yamanaka I, Komatsu T. 1989. Wacker type and π-allyl type oxidations of propylene controlled by fuel cell system in the gas phase. Catal. Lett. 3:365–69
- 112. Winiwarter A, Silvioli L, Scott SB, Enemark-Rasmussen K, Sariç M, et al. 2019. Towards an atomistic understanding of electrocatalytic partial hydrocarbon oxidation: propene on palladium. *Energy Environ.* Sci. 12:1055–67
- Winiwarter A, Boyd MJ, Scott SB, Higgins DC, Seger B, et al. 2021. CO as a probe molecule to study surface adsorbates during electrochemical oxidation of propene. Chem ElectroChem 8:250–56
- Li H, Abraham CS, Anand M, Cao A, Norskov JK. 2022. Opportunities and challenges in electrolytic propylene epoxidation. 7. Phys. Chem. Lett. 13:2057–63
- 115. Green DW, Southard MZ. 2019. Perry's Chemical Engineers' Handbook. New York: McGraw-Hill Educ.
- Mikkelsen M, Jørgensen M, Krebs FC. 2010. The teraton challenge. A review of fixation and transformation of carbon dioxide. *Energy Environ. Sci.* 3:43–81
- Qiao J, Liu Y, Hong F, Zhang J. 2014. A review of catalysts for the electroreduction of carbon dioxide to produce low-carbon fuels. Chem. Soc. Rev. 43:631–75
- Albo J, Alvarez-Guerra M, Castaño P, Irabien A. 2015. Towards the electrochemical conversion of carbon dioxide into methanol. Green Chem. 17:2304–24
- Sarp S, Gonzalez Hernandez S, Chen C, Sheehan SW. 2021. Alcohol production from carbon dioxide: methanol as a fuel and chemical feedstock. *Joule* 5:59–76
- Liu Y, Li F, Zhang X, Ji X. 2020. Recent progress on electrochemical reduction of CO₂ to methanol. Curr. Opin. Green Sustain. Chem. 23:10–17
- Boutin E, Robert M. 2021. Molecular electrochemical reduction of CO₂ beyond two electrons. Trends Chem. 3:359–72
- Zhu G, Li Y, Zhu H, Su H, Chan SH, Sun Q. 2017. Enhanced CO₂ electroreduction on armchair graphene nanoribbons edge-decorated with copper. *Nano Res.* 10:1641–50
- Yang Y, Evans J, Rodriguez JA, White MG, Liu P. 2010. Fundamental studies of methanol synthesis from CO₂ hydrogenation on Cu(111), Cu clusters, and Cu/ZnO(0001). Phys. Chem. Chem. Phys. 12:9909–17
- Canfield D, Frese K Jr. 1983. Reduction of carbon dioxide to methanol on n-and p-GaAs and p-InP Effect of crystal face, electrolyte and current density. J. Electrochem. Soc. 130:1772–73
- Zhang W, Hu Y, Ma L, Zhu G, Wang Y, et al. 2018. Progress and perspective of electrocatalytic CO2 reduction for renewable carbonaceous fuels and chemicals. Adv. Sci. 5:1700275
- Lu L, Sun X, Ma J, Yang D, Wu H, et al. 2018. Highly efficient electroreduction of CO₂ to methanol on palladium-copper bimetallic aerogels. *Angew. Chem. Int. Ed.* 57:14149–53
- Zhang FY, Sheng T, Tian N, Liu L, Xiao C, et al. 2017. Cu overlayers on tetrahexahedral Pd nanocrystals with high-index facets for CO₂ electroreduction to alcohols. *Chem. Commun.* 53:8085–88
- 128. Periasamy AP, Ravindranath R, Senthil Kumar SM, Wu WP, Jian TR, Chang HT. 2018. Facetand structure-dependent catalytic activity of cuprous oxide/polypyrrole particles towards the efficient reduction of carbon dioxide to methanol. *Nanoscale* 10:11869–80
- Albo J, Irabien A. 2016. Cu₂O-loaded gas diffusion electrodes for the continuous electrochemical reduction of CO₂ to methanol. *J. Catal.* 343:232–39
- Zhang W, Qin Q, Dai L, Qin R, Zhao X, et al. 2018. Electrochemical reduction of carbon dioxide to methanol on hierarchical Pd/SnO₂ nanosheets with abundant Pd-O-Sn interfaces. *Angew. Chem. Int. Ed.* 57:9475–79
- Yang D, Zhu Q, Chen C, Liu H, Liu Z, et al. 2019. Selective electroreduction of carbon dioxide to methanol on copper selenide nanocatalysts. *Nat. Commun.* 10:677
- Yang H-P, Qin S, Wang H, Lu J-X. 2015. Organically doped palladium: a highly efficient catalyst for electroreduction of CO₂ to methanol. Green Chem. 17:5144

 –48
- 133. Schizodimou A, Kyriacou G. 2012. Acceleration of the reduction of carbon dioxide in the presence of multivalent cations. *Electrochim. Acta* 78:171–76



- 134. Mahyoub SA, Qaraah FA, Chen C, Zhang F, Yan S, Cheng Z. 2020. An overview on the recent developments of Ag-based electrodes in the electrochemical reduction of CO2 to CO. Sustain. Energy Fuels 4:50-67
- 135. Wu Y, Jiang Z, Lu X, Liang Y, Wang H. 2019. Domino electroreduction of CO2 to methanol on a molecular catalyst. Nature 575:639-42
- 136. Fornaciari JC, Primc D, Kawashima K, Wygant BR, Verma S, et al. 2020. A perspective on the electrochemical oxidation of methane to methanol in membrane electrode assemblies. ACS Energy Lett. 5:2954-63
- 137. Arminio-Ravelo JA, Escudero-Escribano M. 2021. Strategies toward the sustainable electrochemical oxidation of methane to methanol. Curr. Opin. Green Sustain. Chem. 30:100489
- 138. Jiang H, Zhang L, Han Z, Tang Y, Sun Y, et al. 2021. Direct conversion of methane to methanol by electrochemical methods. Green Energy Environ. 7:1132-42
- 139. Luo Y-R. 2007. Comprehensive Handbook of Chemical Bond Energies. Boca Raton, FL: CRC Press
- 140. Heo P, Ito K, Tomita A, Hibino T. 2008. A proton-conducting fuel cell operating with hydrocarbon fuels. Angew. Chem. Int. Ed. 47:7841-44
- 141. Boyd MJ, Latimer AA, Dickens CF, Nielander AC, Hahn C, et al. 2019. Electro-oxidation of methane on platinum under ambient conditions. ACS Catal. 9:7578-87
- 142. Hahn F, Melendres C. 2001. Anodic oxidation of methane at noble metal electrodes: an 'in situ' surface enhanced infrared spectroelectrochemical study. Electrochim. Acta 46:3525-34
- 143. Xie S, Lin S, Zhang Q, Tian Z, Wang Y. 2018. Selective electrocatalytic conversion of methane to fuels and chemicals. J. Energy Chem. 27:1629-36
- Arnarson L, Schmidt PS, Pandey M, Bagger A, Thygesen KS, et al. 2018. Fundamental limitation of electrocatalytic methane conversion to methanol. Phys. Chem. Chem. Phys. 20:11152-59
- 145. Sarno M, Ponticorvo E, Funicello N, De Pasquale S. 2020. Methane electrochemical oxidation at low temperature on Rh single atom/NiO/V2O5 nanocomposite. Appl. Catal. A 603:117746
- 146. Oh C, Kim J, Hwang YJ, Ma M, Park JH. 2021. Electrocatalytic methane oxidation on Co₃O₄incorporated ZrO₂ nanotube powder. Appl. Catal. B 283:119653
- 147. Xu N, Coco CA, Wang Y, Su T, Wang Y, et al. 2021. Electro-conversion of methane to alcohols on "capsule-like" binary metal oxide catalysts. Appl. Catal. B 282:119572
- 148. Kim RS, Surendranath Y. 2019. Electrochemical reoxidation enables continuous methane-to-methanol catalysis with aqueous Pt salts. ACS Cent. Sci. 5:1179-86
- 149. Lee B, Hibino T. 2011. Efficient and selective formation of methanol from methane in a fuel cell-type reactor. J. Catal. 279:233-40
- 150. Tomita A, Nakajima J, Hibino T. 2008. Direct oxidation of methane to methanol at low temperature and pressure in an electrochemical fuel cell. Angew. Chem. Int. Ed. 47:1462-64

Mathison et al.

